
# Comparative analysis of single and multiphase numerical frameworks for subcooled boiling flow in an internal combustion engine coolant jacket

Applied Thermal Engineering 219 (2023) 119435

Contents lists available at ScienceDirect

Applied Thermal Engineering

journal homepage: www.elsevier.com/locate/ate

Research Paper

# Comparative analysis of single and multiphase numerical frameworks for subcooled boiling flow in an internal combustion engine coolant jacket

Sudharsan Vasudevan [a,*], Sassan Etemad [a,b], Lars Davidson [a], Mirko Bovo [c]

[a] Division of Fluid Dynamics Department of Mechanics and Maritime Sciences, Chalmers University of Technology, Hörsalsvägen 7A, Gothenburg SE-412 96, Sweden

[b] Dept. BF93550, AB2 Volvo Technology, Gothenburg SE-40508, Sweden

[c] Aurobay, Powertrain Engineering Sweden AB, Gothenburg, Sweden

ARTICLE INFO

*Keywords:*
Computational fluid dynamics (CFD)
Mixture multiphase
Conjugate heat transfer (CHT)
Subcooled boiling flow
Inter-phase mass transfer
Engine coolant jacket
Precision cooling
Vapor bubble interaction
Enhanced heat transfer

ABSTRACT

Computational analysis of nucleate boiling occurring in liquid cooled applications, such as internal combustion engines is often implemented within a single phase Computational Fluid Dynamics (CFD) framework, owing to low vapor fractions involved. With increase in specific power and the resulting higher thermal loads, accounting for the presence of the vapor phase using a multiphase framework is required in certain conditions, despite the higher computational costs. While detailed resolution of the liquid and vapor phases in nucleate boiling using a two fluid model is excessively computationally expensive, the homogeneous mixture multiphase framework is a good compromise between resolution and computational cost. In this article a numerical wall boiling model is implemented within both, a single phase and the mixture multiphase frameworks. Results from the two approaches are compared with measurements in a channel flow. The results from both approaches are in good agreement with experiments. The single phase approximation is valid when the vapor generation is low. The sensitivity of the results to the computational grid is also discussed in detail. Further, the two frameworks are used to simulate the heat transfer in the coolant jacket of a four-cylinder petrol engine. The results from the numerical simulations are compared with measurements. Both computational frameworks compare reasonably well with the measurements in terms of local metal temperature. However, the advantage of accounting for the vapor phase using the mixture multiphase framework is evident when the parameter related to vapor bubble interactions is analyzed in detail.

## 1. Introduction

Subcooled boiling flow entails exponential increase in heat transfer compared to heat transfer by single phase forced convection only. This is primarily due to formation of vapor bubbles and their interaction with the bulk flow of the coolant. Both single phase and multiphase modeling frameworks in Computational Fluid Dynamics (CFD) are used for numerical analysis of subcooled boiling flow. The single phase framework demands lesser computational efforts compared with the multiphase frameworks. The single phase framework provides reasonably accurate results when the net vapor generated is low. However, when there is an increase in amount of vapor generated, there is a risk of increasing the liquid temperature to unphysically high values, especially in the near-wall cells. This is because the latent heat of vaporization during the phase change process is not accounted for in the single phase framework.

Implementation of numerical boiling models within multiphase frameworks, especially using a two-fluid approach, is more accurate than the single phase framework in capturing the effects of vapor bubbles' formation and their interaction with the bulk flow. Hua et al. [1] simulated boiling in engine coolant jacket passages using a two-fluid approach coupled with the Rensselaer Polytechnic Institute (RPI) wall boiling model [2]. In such simulations, the transport equations for mass, momentum and energy are solved independently for the two phases in transient mode, in addition to transport equations for volume fraction of the phases. The results obtained were in really good agreement with results from experiments on simple geometries and engine tests. However, these simulations are computationally expensive, as the number of transport equations solved increases significantly compared to the single-phase framework. The homogeneous mixture multiphase framework is presented as a good compromise between accuracy and computational effort. In this framework, the transport equations of mass, momentum and energy are solved for a mixture phase, along with transport equations for volume fraction of the phases. Thereby,

* Corresponding author.
*E-mail address:* sudharsan.vasudevan@chalmers.se (S. Vasudevan).

https://doi.org/10.1016/j.applthermaleng.2022.119435
Received 29 April 2022; Received in revised form 19 August 2022; Accepted 30 September 2022
Available online 12 October 2022

the computational effort is considerably reduced, compared with a two-fluid approach, while still accounting for the presence of the vapor phase. A brief review of studies employing the mixture multiphase approach for automotive cooling applications is presented below.

Bo [3] modeled the effects of local boiling in engine coolant jacket passages using the Rohsenow's wall boiling model [4] within a mixture multiphase framework. In this study, a model for interphase mass transfer, based on the liquid and vapor phase enthalpies, was used. The results were validated with measurements on simple geometries and then the numerical methodology was applied to an engine coolant jacket. Przulj and Shala [5] and Shala [6] used a modified version of the RPI wall boiling model within the mixture multiphase framework to study subcooled boiling flow in engine coolant jacket. They concluded that modeling the fluid as a homogeneous mixture to analyze nucleate boiling provides a good compromise between accuracy and computational efficiency. Punekar and Das [7], Das and Punekar [8] also highlighted the significance of such a modeling approach for boiling based cooling systems. They used a modified version of Chen's correlation within the mixture multiphase framework to study nucleate boiling in an Exhaust Gas Recirculation (EGR) cooler [8]. From these studies, it is evident that several boiling models have been implemented within the versatile mixture multiphase framework in order to analyze heat transfer in boiling based cooling systems.

In this article the Blended Boiling Model, BBM, proposed by Vasudevan et al. [9] is implemented within a single phase and the mixture multiphase frameworks to study subcooled boiling flow. In the multiphase framework, the interphase mass transfer model proposed by Bo [3] is used. In addition to the wall heat flux, the BBM also provides information about bubble radii and probability of bubble interactions. These quantities form the basis for detailed analysis of results from the numerical simulations. The results from the simulations are validated with channel flow measurements by Steiner et al. [10]. Further, the sensitivity of the results to resolution of the computational grid is discussed in detail. The numerical methodology is then applied to study the heat transfer in the coolant jacket of a four-cylinder petrol engine. The results are compared with data obtained from engine rig tests. The commercial Computational Fluid Dynamics (CFD) software Star-CMM+ is used for the numerical simulations.

## 2. Numerical modeling

In this section, the governing equations of mass, momentum and energy are given. Further, the model for interphase mass transfer used in the mixture multiphase framework is also described, followed by a brief description of the boiling model.

### 2.1. Governing equations

The transport equations for mass, momentum and energy in the mixture multiphase framework are identical to the single phase framework, except that they are expressed for the mixture phase, here indicated with the subscript '$m$'. In the mixture multiphase framework, transport equations for volume fraction of the two phases are solved, in addition to the transport equations for mass, momentum and energy.

The transport equation for mass of the mixture phase, in the absence of a source term, reads,

$$\frac{\partial}{\partial t}(\rho_m) + \vec{\nabla}.(\rho_m \vec{V}_m) = 0 \tag{1}$$

The mixture density, $\rho_m$, is a volume weighted average of the densities of the liquid phase, $\rho_l$, and vapor phase, $\rho_v$. The mixture velocity, $\vec{V}_m$, is a density weighted average of the velocity of the constituting phases. The expressions for $\rho_m$ and $\vec{V}_{\vec{m}}$ are given below.

$$\rho_m = \alpha_l \rho_l + \alpha_v \rho_v \tag{2}$$

$$\vec{V}_m = x_l \vec{V}_l + x_v \vec{V}_v \; ; \quad x_i = \frac{\rho_i}{\rho_m}\alpha_i, \; i = \{l, v\} \tag{3}$$

where, $\alpha_i$ and $x_i$ are the volume fraction and mass fraction, respectively, of the individual phases constituting the mixture and the subscripts '$l$' and '$v$' correspond to liquid and vapor, respectively. From the continuity equation for the mixture phase, the transport equation for volume fraction of the individual phases can be obtained. The equations read

$$\frac{\partial}{\partial t}(\alpha_l) + \vec{\nabla}.(\alpha_l \vec{V}_m) = Su_{\alpha,l} \tag{4}$$

$$\frac{\partial}{\partial t}(\alpha_v) + \vec{\nabla}.(\alpha_v \vec{V}_m) = Su_{\alpha,v}. \tag{5}$$

Note that the source terms in the volume fraction equations, $Su_{\alpha,l}$ and $Su_{\alpha,v}$, have the units $s^{-1}$.

The transport equation for momentum of the mixture phase reads,

$$\frac{\partial}{\partial t}(\rho_m \vec{V}_m) + \vec{\nabla}.(\rho_m \vec{V}_m \vec{V}_m) = -\vec{\nabla} P + \vec{\nabla}\overline{\overline{T}}_m + \vec{f}_b + S_{u,mom}. \tag{6}$$

Here, $P$ denotes the pressure, $\overline{\overline{T}}_m$ denotes the viscous stress tensor and $\vec{f}_b$ denotes body force. Any other source to the momentum equation is accounted for in the $S_{u,mom}$ term. The transport equation for total energy of the mixture phase, $E_m$, reads,

$$\frac{\partial}{\partial t}(\rho_m E_m) + \vec{\nabla}.(\rho_m E_m \vec{V}_m) = \vec{\nabla}.\vec{q} - \vec{\nabla}.(P\vec{V}_m) + \vec{\nabla}.(\overline{\overline{T}}_m \vec{V}_m) + S_{u,E_m} \tag{7}$$

The blended wall functions available in Star-CCM+ are used for the near wall treatment. The wall function for estimating the non-dimensional velocity in the near wall cell is given by

$$u^+ = \frac{1}{\kappa}\ln(1+\kappa y^+) + C\left(1 - e^{-y^+/y_m^+} - \frac{y^+}{y_m^+}e^{-by^+}\right) \tag{8}$$

$$C = \frac{1}{\kappa}\ln\left(\frac{E'}{\kappa}\right) b = \frac{1}{2}\left(y_m^+ \frac{\kappa}{C} + \frac{1}{y_m^+}\right) \tag{9}$$

$$E' = \frac{E}{f} \tag{10}$$

where $y_m^+$ corresponds to the theoretical intersection of the solutions of the viscous sub-layer and the log-layer. The von Karman constant is denoted by $\kappa$, the log law offset is denoted by $E$ and $f$ is a roughness function.

The wall function for estimating the non-dimensional temperature reads,

$$T^+ = exp(-\Gamma)Pry^+ + exp(-\frac{1}{\Gamma})Pr_t\left[\frac{1}{\kappa}\ln(E'y^+) + P'\right] \tag{11}$$

$$\Gamma = \frac{0.01c(Pry^+)^4}{1 + \frac{5}{c}Pr^3 y^+} \tag{12}$$

$$c = exp(f-1) \tag{13}$$

where $Pr$ and $Pr_t$ are the Prandtl number and turbulent Prandtl number, respectively. The term $P'$ governs the velocity at which the log-layer and the viscous sub-layer of the thermal profiles intersect. The reader is referred to the Star-CCM+ user guide for further details [11].

In Star-CCM+, when using the mixture multiphase framework, the energy equation is recast to a simple convection–diffusion equation to solve for temperature as the transported variable. Once the temperature is solved for, the enthalpies of the liquid phase, $h_l$, and the vapor phase, $h_v$, are estimated using the equations given below.

$$h_l = h_{l,ref} + \int_{T_{ref}}^{T} c_l dT \tag{14}$$

$$h_v = h_{v,ref} + \int_{T_{ref}}^{T} c_v dT \tag{15}$$

$$h_m = x_l h_l + x_v h_v \tag{16}$$

where, $c_l$ and $c_v$ are specific heat of the liquid phase and the vapor phase, respectively. The reference enthalpies of the liquid phase, $h_{l,ref}$, and the vapor phase, $h_{v,ref}$, are specified at the reference temperature $T_{ref}$.

The standard two-layer $k\epsilon$-model is chosen for modeling the turbulence. The two-layer option provides an all-$y^+$ wall treatment, where the model automatically switches between resolving the viscous sub layer and using wall functions, in the near-wall cell, based on the local value of wall $y^+$.

### 2.2. Interphase mass transfer model

The model for interphase mass transfer forms an integral part of the numerical methodology in the mixture multiphase framework. The model estimates the amount of liquid evaporating close to the wall and the amount of vapor condensing in the liquid bulk. The model for interphase mass transfer proposed by Bo [3] is used in the present study. The mass transfer between the phases is based on the mixture specific enthalpy, $h_m$. First, a vapor volume fraction corresponding to a reduced thermal equilibrium condition is evaluated as

$$\overline{\alpha_v} = \frac{x_{v,eq}^n}{x_{v,eq} + (1 - x_{v,eq})\frac{\rho_v}{\rho_l}} \; ; \; n = 1.1 \tag{17}$$

where $x_{v,eq}$ is the mass fraction of vapor computed based on thermal equilibrium conditions.

$$x_{v,eq} = \begin{cases} 0, \text{if } h_m \le h_{l,sat} \\ \frac{h_m - h_{l,sat}}{h_{lv}}, \text{if } h_{l,sat} < h_m < h_{v,sat} \\ 1, \text{if } h_m \ge h_{v,sat} \end{cases} \tag{18}$$

where $h_{l,sat}$ is the saturation enthalpy of the liquid phase, $h_{v,sat}$ is the saturation enthalpy of the vapor phase and $h_{lv} (= h_{v,sat} - h_{l,sat})$ is the latent heat of vaporization. The values of enthalpy at saturation conditions are estimated as

$$h_{l,sat} = h_{l,ref} + \int_{T_{ref}}^{T_{sat}} c_l dT \tag{19}$$

$$h_{v,sat} = h_{v,ref} + \int_{T_{ref}}^{T_{sat}} c_v dT \tag{20}$$

The actual vapor volume fraction in a computational cell is compared with the reference value computed from Eq. (17). The difference between the two values is the driving force for evaporation or condensation. From this, the source term $Su_{\alpha,v}$ in the vapor volume fraction equation, Eq. (5), is computed as given below.

$$Su_{\alpha,v} = \omega_{evap} + \omega_{cond} \tag{21}$$

where $\omega_{evap}$ and $\omega_{cond}$ are volume fraction sources arising from the evaporation and condensation, respectively. These terms are computed as follows.

$$\omega_{evap} = \begin{cases} \frac{\overline{\alpha_v} - \alpha_v}{t_{evap}}, \text{if } \alpha_v < \overline{\alpha_v} \\ 0, \text{if } \alpha_v \ge \overline{\alpha_v} \end{cases} \tag{22}$$

$$\omega_{cond} = \begin{cases} \frac{\overline{\alpha_v} - \alpha_v}{t_{cond}}, \text{if } \alpha_v > \overline{\alpha_v} \\ 0, \text{if } \alpha_v \le \overline{\alpha_v} \end{cases} \tag{23}$$

In the above equations, $t_{evap}$ and $t_{cond}$ are the time scales required for $\alpha_v$ to reach $\overline{\alpha_v}$ through evaporation and condensation, respectively. While $t_{evap}$ is a constant value, the expression for $t_{cond}$, which is based on the degree of subcooling in a cell, reads,

$$t_{cond} = K_{cond} \frac{T_{sat}}{\Delta T_{sub}} \; ; \; \Delta T_{sub} = T_{sat} - T \tag{24}$$

where $\Delta T_{sub}$ is the subcooling and $K_{cond}$ is a constant with units $s$. The values $K_{cond} = t_{evap} = 5$ are used in this study. The source term in the transport equation for volume fraction of the liquid, $Su_{\alpha,l}$, is the negative of $Su_{\alpha,v}$. It is to be noted that, although the mixture multiphase framework accounts for the presence of the vapor phase, a dedicated boiling model is still essential for accounting for the additional heat transfer due to boiling at the solid–liquid interface.

When boiling occurs, the heat flux between wall and near wall cell is dominated by the phase change phenomena. In the single phase framework, which does not account for phase change, this heat flux translates to an increase in the cell internal energy and can lead to the cell temperature exceeding the wall temperature. To avoid this unphysical result, the boiling component of the heat flux from the wall is limited by multiplying it with a suppression factor that is based on the temperature in the near wall cell ($T_{cell}$). The expression for the suppression factor reads,

$$SF = \min\left[1, \max\left(0, \frac{T_{wall} - T_{cell}}{T_{wall} - T_{sat}}\right)\right]. \tag{25}$$

Such a term is not required in the multiphase framework since the vaporization enthalpy is accounted for and it limits the near wall cell temperature. For further details about implementation of boiling models and models for interphase mass transfer in Star-CCM+, the reader is referred to Star-CCM+ documentation [11].

### 2.3. Boiling model

The Blended Boiling Model, BBM, proposed by Vasudevan et al. [9] is used in the present study to model subcooled flow boiling. The model has been implemented using the 'user code' functionality in Star-CCM+. The model blends the Boiling Departure Lift-off model proposed by Steiner et al. [10] and the Rohsenow's pool boiling correlation [4]. The BDL model estimates the heat flux in the isolated bubbles regime and the Rohsenow's correlation estimates the heat flux in the Fully Developed Boiling (FDB) regime. The blending parameter in the BBM, which estimates the probability of bubble interaction, accounts for the increase in vapor bubble population from the isolated bubbles regime to the FDB regime. The total wall heat flux, $q_{wall}$, estimated by the BBM reads,

$$q_{wall} = (1 - \Pi) q_{BDL} + \Pi q_{Roh} \; ; \; 0 \le \Pi \le 1 \tag{26}$$

where, $q_{BDL}$ is the heat flux estimated by the BDL model, $q_{Roh}$ is the heat flux estimated by Rohsenow's correlation and $\Pi$ denotes the probability of bubble interaction, which is the blending parameter. The expression for heat flux estimated using the BDL model reads,

$$q_{BDL} = q_{fc} + S_{flow} S_{subcool} q_{nb} \; ; \; 0 \le S_{flow} S_{subcool} \le 1. \tag{27}$$

The BDL model, in Eq. (27), is based on the heat flux partitioning approach. The total heat flux is a sum of the single phase forced convection heat flux, $q_{fc}$ and the nucleate boiling heat flux, $q_{nb}$. The nucleate boiling heat flux is estimated using the correlation proposed by Foster and Zuber [12]. In the formulation of the BDL model, the nucleate boiling part involves two suppression factors, $S_{flow}$ and $S_{subcool}$, which account for the flow-induced and subcooling-induced suppression of nucleate boiling, respectively [10].

The Rohsenow's pool boiling correlation reads,

$$q_{Roh} = \mu_l h_{lv} \sqrt{\frac{g(\rho_l - \rho_v)}{\sigma}} \left( \frac{c_l \Delta T_{sat}}{C_{sf} h_{lv} Pr_l^{n_p}} \right)^m \tag{28}$$

where the thermophysical properties of the liquid, such as the dynamic viscosity, density, specific heat and Prandtl number, are denoted by $\mu_l$, $\rho_l$, $c_l$ and $Pr_l$, respectively. Surface tension is denoted by $\sigma$, latent heat of vaporization by $h_{lv}$ and vapor density by $\rho_v$. Three empirical constants appear in the Rohsenow's correlation: $C_{sf}$, $n_p$ and $m$. The constants depend on the liquid coolant and material of the solid heater used. The blending parameter, $\Pi$, is the probability of occurrence of more than one vapor bubble nucleating on the heated surface within the area, $A_c$. This area $A_c$ is estimated based on two times the bubble departure diameter, which is computed in the BDL model. An essential part of estimating the blending parameter is the active nucleation site density $N$, which is the number of nucleation sites per unit area. The expression for $\Pi$ reads,

$$\Pi = 1 - \exp(-N A_c). \tag{29}$$

The active nucleation site density, $N$, is estimated using the model proposed by Li et al. [13]. The expression for active nucleation site density reads

$$N = N_0(1-\cos\phi)\exp(f(P))\Delta T_{sat}^{A\Delta T_{sat}+B} \tag{30}$$

with

$$f(P) = 26.006 - 3.678\exp(-2P) - 21.907\exp\left(\frac{-P}{24.065}\right) \tag{31}$$

$$A = -0.0002P^2 + 0.0108P + 0.0119 \tag{32}$$

$$B = 0.122P + 1.988 \tag{33}$$

$$1-\cos\phi = (1-\cos\phi_0)\left(\frac{T_c - T_{sat}}{T_c - T_0}\right)^{\Gamma} \tag{34}$$

where $N_0$ is an empirical constant that scales the number of active nucleation sites, $P$ is the pressure expressed in MPa, $\phi$ is the contact angle, $T_c$ is the critical temperature at which the contact angle becomes zero, $T_0$ is the reference temperature and $\phi_0$ is the contact angle corresponding to the reference temperature. The default values suggested by Li et al. [13], $\phi_0 = 41.37°$ at $T_0 = 25$ °C, and $\Gamma = 0.719$, are used in this study.

According to Eq. (29), the value of $\Pi$ asymptotically approaches a value of 1 with increase in number of active vapor bubble nucleation sites, $N$. In line with this, in Eq. (27), a non-zero value of $\Pi$ signifies the end of the isolated bubbles regime and a value of $\Pi \simeq 1$ signifies occurrence of FDB. Once FDB is encountered, any increase in input heat load would result in occurrence of critical heat flux which eventually leads to transition and film boiling regimes, which are detrimental to the component being cooled. The blending parameter $\Pi$ informs the proximity to FDB, and it can be used to restrict boiling within safe limits in practical applications. For further details about the BBM, the reader is referred to the article by Vasudevan et al. [9].

## 3. Results and discussion

The first part of this section is a detailed discussion of results from the numerical simulations of a rectangular-sectioned channel flow with a heater at its bottom surface. The data from experimental studies by Steiner et al. [10] is used to validate the numerical simulations. In the second part of this section, the results from Computational Fluid Dynamics - Conjugate Heat Transfer (CFD-CHT) simulations of a four-cylinder petrol engine are presented and are compared with results from engine rig tests.

### 3.1. Subcooled boiling flow in a channel

Steiner et al. [10] experimentally investigated subcooled boiling flow in a rectangular-sectioned channel. In their test setup, the material of the heated surface was an aluminum alloy and the coolant used was water. The primary test section was 30 mm wide and 40 mm high. The information provided by Prof. Steiner [14] were used to obtain the right inlet flow conditions to the primary test section. A flow development section and a transition section were installed upstream of the primary test section. The flow development section was a $3m$ long pipe, circular in cross-section with a diameter of 40 mm. The transition section was 200 mm long and has a circular cross-section at its inlet and a rectangular cross section at its outlet. The primary test section itself was 155 mm long. The arrangement is shown in Fig. 1. The test specimen was mounted flush with the bottom surface of the channel at a distance of 45 mm from its inlet. The face of the test specimen in contact with the coolant had a length of 60 mm in the stream-wise direction and a width of 10 mm in the span-wise direction. The coolant flow velocity and the operating pressure of the cooling system were varied to obtain a series of wall heat flux vs. wall temperature curves. The operating conditions in the experiments are summarized in Table 1.

**Table 1**
Operating conditions in experiments by Steiner et al. [10]. Maximum wall temperature limited to 160 °C.

| Liquid bulk temperature $T_{bulk}$ [°C] | Operating pressure P [bar] | Bulk velocity $v_{bulk}$ [m/s] | Saturation temperature $T_{sat}$ [°C] |
|---|---|---|---|
| 95.0 | 1.5 | 0.05, 0.39, 1.17 | 111.35 |
| 95.0 | 2.0 | 0.20, 0.39, 1.17 | 120.21 |

In the CFD simulations, the fully developed flow in the flow development section is obtained by simulating an infinitely long circular-sectioned pipe. This is done by modeling a short circular-sectioned pipe with periodic boundary condition specified at its inlet and outlet surfaces, meaning that the outlet flow is fed back into the inlet. The transition section and the primary test section were modeled as one entity. The velocity profile from the development section was mapped onto the inlet of the transition section in order to obtain the right inlet flow conditions. The results from steady-state simulations using both the single phase and the mixture multiphase frameworks are presented along with the results from the experiments in Fig. 2. Wall functions are used to model the transported quantities in between the near-wall cell and the wall.

As can be seen, for the case with the lowest bulk velocity, $v_{bulk} = 0.05$ m/s, in Fig. 2, the heat flux estimated by the single phase framework is significantly lower than the one estimated by the mixture multiphase framework. This is because, the low bulk velocity allows intense boiling with significant amount of vapor generation. Since the single phase framework does not account for the latent heat of vaporization, the near-wall cell temperature increases monotonically. As a remedy for this issue, the suppression factor, shown in Eq. (25), limits the heat transfer from the wall and thereby ensures the temperature in the near wall cell does not exceed the temperature at the wall. Consequently, the heat flux is underestimated by the single phase framework. In the absence of the suppression factor, the liquid temperature in the near wall cell would exceed the wall temperature, which would not be physically correct. However, for larger bulk velocities and the consequent decrease in intensity of boiling, the results from the single phase and multiphase frameworks are identical. An over-prediction of wall heat flux for the maximum bulk velocity case ($v_{bulk} = 1.17$ m/s) corresponding to both values of pressure is observed in both frameworks. This over-prediction is not boiling model dependent and stems from the over-prediction of the single phase forced convection heat flux. This is specifically evident for the case with $P = 2.0$ bar and high velocity, where the over-prediction is clearly evident for wall temperatures below the saturation temperature of 120 °C. In support of this argument, the convective heat flux in the BBM is estimated using the standard Dittus–Boelter correlation [15] (instead of using wall functions in CFD) and the results corresponding to the high velocity case, i.e., $v_{bulk} = 1.17$ m/s, are presented in Fig. 3 . The agreement with the experimental results in Fig. 3 is better than that in Fig. 2. However, the over-prediction of convection heatflux by CFD, in Fig. 2, could not be explained.

This study includes also a grid sensitivity analysis of the mixture multiphase framework. For the case with $v = 0.2$ m/s at an operating pressure of 2.0 bar, Fig. 4 shows the results from the grid sensitivity analysis. It is evident from Fig. 4 that the heat flux is over-predicted for the refined mesh, with average wall $y^+ = 1.8$. For such low values of wall $y^+$, the wall function is not used and the viscous sub layer is resolved instead. The results with other mesh configurations agree well with the experiments. The over-prediction can be explained using the expression for the conductive heat flux ($q_{cond}$) from the wall surface to the near-wall fluid cell, which reads,

$$q_{cond} = -k_l\frac{T_{wall} - T_{cell}}{\Delta y} \tag{35}$$

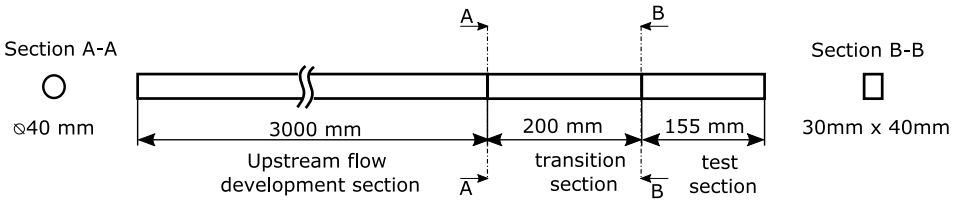


**Fig. 1.** Arrangement of the flow development section, transition section and the primary test section in the experiments by Steiner et al. [10]. The arrangement depicted is based on information from Prof. Steiner [14].

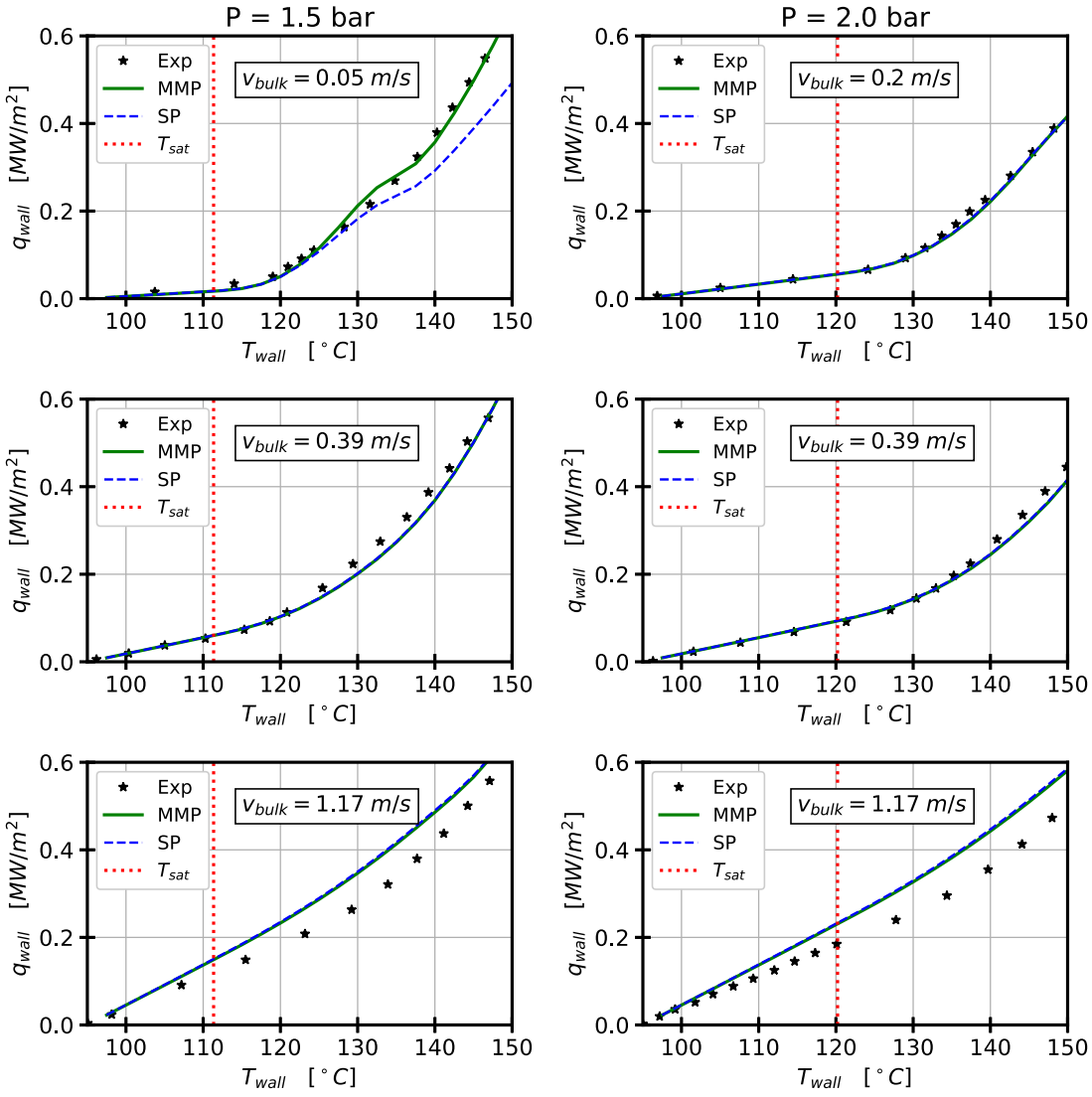


**Fig. 2.** Wall heat flux vs. wall temperature plots comparing results from the mixture multiphase (MMP) and single phase (SP) simulations with the experiments.

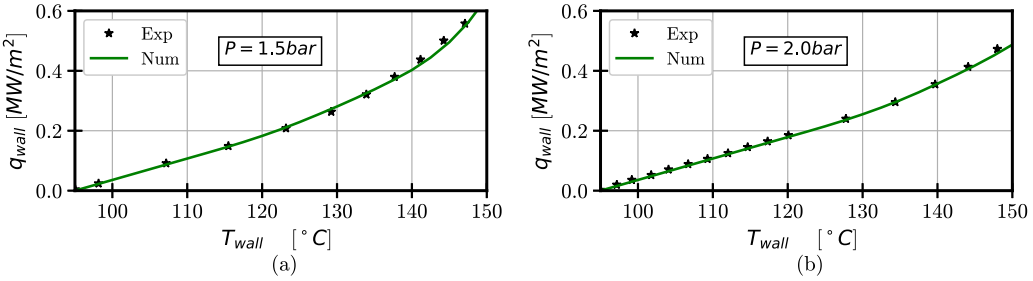


**Fig. 3.** Wall heat flux vs. wall temperature plots for $v_{bulk}$ = 1.17 m/s with the convective heat transfer estimated using Dittus–Boelter correlation corresponding to an operating pressure of (a) 1.5 bar and (b) 2.0 bar.

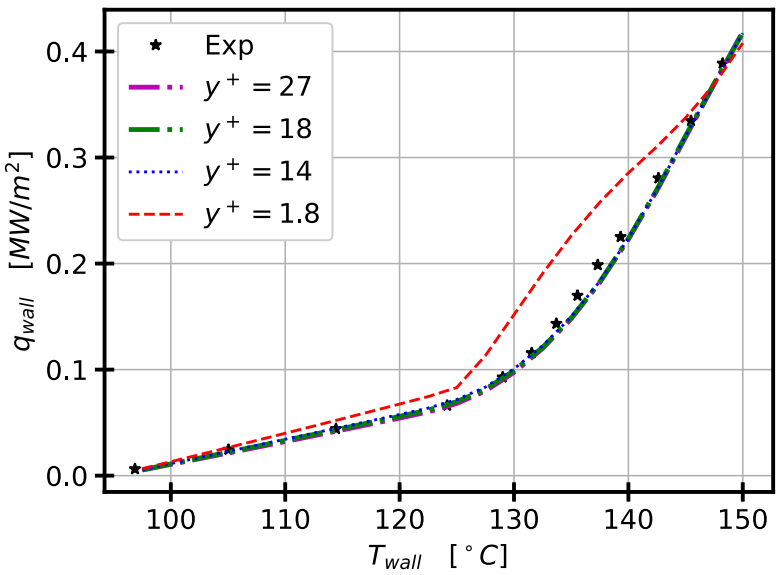


**Fig. 4.** Wall heat flux vs. wall temperature plots comparing results from different computational meshes using the mixture multiphase framework for the $v = 0.2$ m/s case at an operating pressure of 2.0 bar.

where $k_l$ is the liquid thermal conductivity and $\Delta y$ is the distance between the wall and the near-wall cell center. Eq. (35) is solved when the viscous sublayer is resolved. When using the multiphase framework, the interphase mass transfer model limits the temperature of the near wall cell to the saturation temperature. Thereby, the difference in temperature between the wall cell and the near-wall cell, $T_{wall} - T_{cell}$, is replaced by $T_{wall} - T_{sat}$. When the grid is refined the heat flux, $q_{cond}$, increases as the numerator remains constant while the denominator, $\Delta y$, decreases for finer and finer grids, as can be seen from Eq. (35). It is also evident from Fig. 4 that the wall heat flux agrees quite well with the experiments for higher wall temperatures, i.e., $T_{wall} \geq 140$ °C, for the refined mesh. However, this is due to an unphysical increase in the temperature of the near wall cell caused by insufficient vapor generated. To explain this in further detail, the effect of varying the constant $t_{evap}$, shown in Eq. (22), is studied below.

The refined mesh configuration, i.e., $y^+ = 1.8$, where the heat flux is estimated incorrectly, is considered for this study. The results are presented in Fig. 5. The plots of wall heat flux vs. wall temperature obtained for different values of $t_{evap}$ are shown in Fig. 5(a). The maximum temperature occurring in the near wall cells is shown in Fig. 5(b). As can be seen from Fig. 5(b), the near wall cell temperature for the default value of $t_{evap} = 5.0$ increases with increasing wall temperature. In fact, this value even marginally exceeds the wall temperature at $T_{wall} = 150$ °C. This is clearly due to increase in temperature resulting from insufficient vapor generated in those cells. This effect is exaggerated when the value of $t_{evap}$ is increased to 10. This is because, an increase in $t_{evap}$ causes decrease in $\omega_{evap}$ in Eq. (22). A decrease in $\omega_{evap}$ in turn leads to a decrease in the source term, $Su_{\alpha,v}$, in the transport equation for volume fraction of the vapor phase, shown in Eq. (21). To reduce this effect, the value of $t_{evap}$ is reduced in an effort to generate enough vapor to ensure the temperature in the near-wall cell does not increase unphysically. For a value of $t_{evap} = 1s$ the near wall cell temperature is close to the saturation temperature of $T_{sat} = 120.2$ °C corresponding to the operating pressure of 2.0 bar. For this case, the heat flux, shown in Fig. 5(a), is over-estimated and this is attributed to the high temperature gradient in between the wall cell and the near-wall cell, as described previously using Eq. (35).

Furthermore, the mixture multiphase framework, for simulating nucleate boiling, is formulated based on volume averaging of the liquid and vapor phases. The sample volume for averaging should be large enough in order to ensure representative averaging within the cell. In nucleate boiling, vapor bubbles grow on the surface until they become large enough to detach and condense in the bulk flow. Fig. 6 shows the ratio of bubble departure diameter, at the instant of detachment of vapor bubble from its nucleation site, to the height of the near-wall cell as a function of wall temperature for the mesh refinements investigated. It is to be noted that the bubble departure diameter is the one computed in the BDL model. Clearly, the vapor bubble diameter is larger than the height of the near-wall cell, $d/\Delta y > 1$, for the excessively refined mesh, returning inaccurate results. This is not the case in other mesh configurations. Thereby, the level of grid refinement can be limited by comparing the height of the near-wall cell with the characteristic bubble diameter for a given operating condition.

Based on discussions presented, refining the computational mesh excessively to resolve the transported quantities in the viscous sub layer proves to be counter-productive while using the mixture multiphase framework for subcooled boiling flow. This is also in line with the observations of Punekar and Das [7], where the Chen's boiling model was implemented within the mixture multiphase framework and was validated with experimental data of Robinson et al. [16]. They mention that wall function treatment for near wall boundary layer was chosen since refining the mesh does not produce solutions of interesting accuracy. Furthermore, excessive grid refinement in a single phase framework will also lead to counter-productive results. In this case, if the resolved near wall cell temperature is higher than the saturation temperature of the liquid, the boiling suppression shown in Eq. (25) is activated and limits the heat transfer from the wall. Hence, intentional near wall mesh refinement is avoided to analyze subcooled flow boiling in the coolant jacket of a four-cylinder petrol engine in the forthcoming section.

### 3.2. Subcooled flow boiling in a four-cylinder petrol engine

In this section the single phase and the multiphase frameworks are compared when applied to analyze heat transfer in an actual engine coolant jacket. The results are compared with measurements from rig tests.

#### 3.2.1. Engine rig tests

Tests are conducted on a four-cylinder petrol engine installed in a test cell with conditioned environment. The engine driven mechanical coolant pump is replaced with an electric pump in order to arbitrarily control the coolant flow rate. Engine tests replacing the engine driven coolant pump with an electric pump have been conducted in the past.

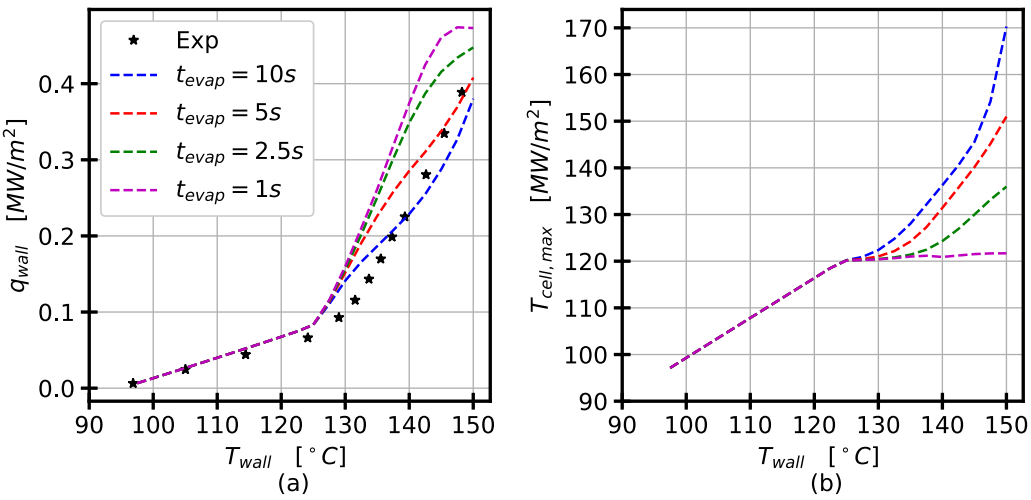


**Fig. 5.** (a) Wall heat flux vs. wall temperature plots presenting the effect of the constant $t_{evap}$. (b) Maximum temperature in the near-wall cell vs. wall temperature. The results are obtained using the mixture multiphase framework for the $v = 0.2$ m/s case at an operating pressure of 2.0 bar.

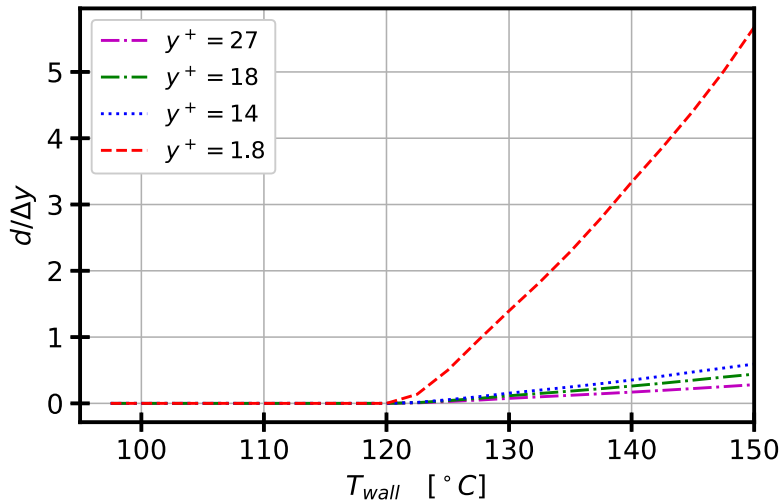


**Fig. 6.** Ratio of bubble diameter at the instant of vapor bubble departure to the height of the near-wall cell vs. wall temperature. The results are obtained using the mixture multiphase framework for the $v = 0.2$ m/s case at an operating pressure of 2.0 bar.

One such test was reported by Finley et al. [17] where the coolant pump was controlled using an electric motor in order to study the factors influencing combustion chamber wall temperature, such as cylinder head material, coolant composition, coolant flow rate, etc. In this article, the results from the thermal survey measurement campaign reported by Båstedt et al. [18] are used for evaluation of the numerical methodology. During the tests, the coolant flow rate and the operating pressure of the cooling system are varied systematically to study boiling occurring in the coolant jacket. The coolant bulk temperature at the inlet is 100 °C. It is worth highlighting that the coolant flow rates in these tests, including the maximum (100%) case, are lower than the flow rate delivered by the engine driven mechanical pump used in the engines in production. In order to measure local metal temperature, thermocouples are placed at several locations in the engine cylinder head which are considered critical from the point of view of boiling. These locations include the region between the two exhaust valves, known as the exhaust valve bridge, and the region in the vicinity of the exhaust flange of the Integrated Exhaust Manifold (IEM), both shown in Fig. 7. Results from numerical simulations are compared with temperatures measured in these two regions.

### 3.2.2. Numerical modeling

A high-resolution three dimensional Computational Fluid Dynamics-Conjugate Heat Transfer (CFD-CHT) model used at Aurobay is made available to this study. The boundary conditions in the CFD-CHT model are set in line with the operating conditions of the rig tests. The computational domain consists of the entire base engine structure, constituting the solid domain, and the coolant jacket, constituting the fluid domain. Heat transfer by conduction is solved for in the solid part of the domain. The in-cylinder combustion and the resulting hot gases are the heat source. On the walls exposed to the heat source, heat transfer coefficient and reference temperature from the in-cylinder combustion and gas-side CFD simulations are mapped as boundary conditions in the model. The heat sinks are the coolant, the oil and the ambient air in the test cell. The heat transfer to the coolant in the coolant jacket is resolved. On the walls exposed to other heat sinks, a convective boundary condition is implemented specifying the heat transfer coefficient and the reference temperature. The engine coolant jacket has one inlet and two outlets, shown in Fig. 8. While the main outlet opens to the thermostat valve, the other outlet diverts coolant flow to the cabin heater. The coolant bulk temperature and mass flow

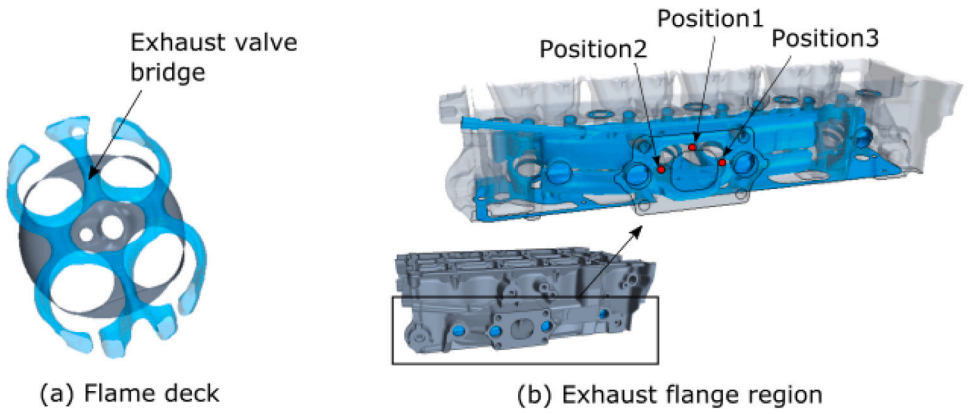


**Fig. 7.** The geometry of the engine in the vicinity of (a) the flame deck (shown in gray) with the exhaust valve bridge indicated, the coolant jacket (shown in blue) (b) exhaust flange showing position of thermocouples. Surface of the coolant jacket is highlighted in blue color.

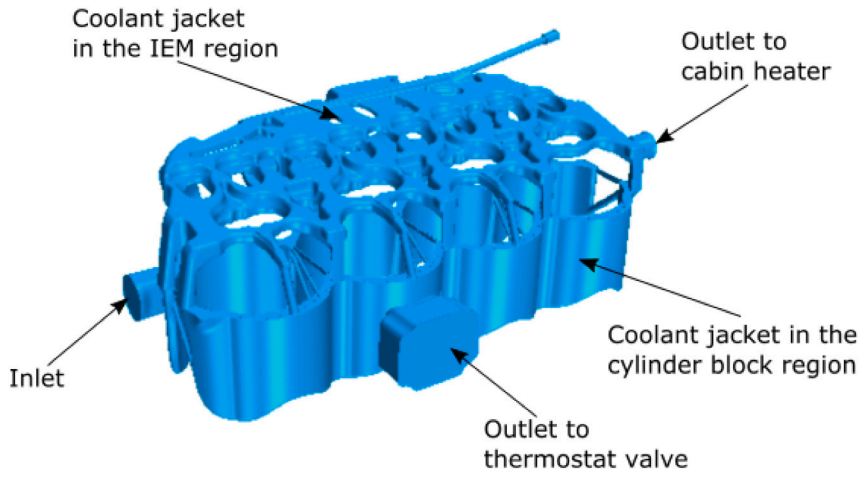


**Fig. 8.** Coolant jacket geometry in the cylinder block and Integrated Exhaust Manifold (IEM) regions with the inlet and the outlets indicated.

rate are specified at the inlet. Pressure is specified at the main outlet, to set the correct system pressure, while mass flow is set to the secondary outlet to ensure that the flow split between the outlets corresponds to the measurements. The commercial CFD code Star-CCM+ is used for the computations. The CFD-CHT model is meshed with polyhedral cells with 7.6 million cells in the fluid part of the domain and 25.7 million cells in the solid part of the domain.

### 3.2.3. *Results: Four-cylinder petrol engine*

Fig. 9 shows local metal temperature vs. coolant pressure plots measured in the vicinity of the exhaust valve bridge of Cylinder 4 during the rig tests. Firstly, a decrease in temperature with reduction in coolant pressure is observed and interpreted as occurrence of boiling. The saturation temperature of the coolant decreases with reduction in system pressure and thereby promotes boiling. Since heat transfer by boiling is significantly higher than that by forced convection alone, the metal temperature decreases. Secondly, an increase in temperature is observed with a reduction in coolant flow rate. A reduction in coolant flow rate, at constant inlet bulk temperature, results in an increased coolant outlet temperature and thereby an increased average coolant temperature in the engine. This, consequently, results in an increase in overall temperature levels in the engine. Simultaneously, a reduction in coolant flow rate results in a decrease in convective heat transfer coefficient. This further contributes to the solid temperature increase. Similar behavior is observed in the exhaust valve bridge of the other three cylinders.

Four operating conditions are marked in Fig. 9 for which numerical simulations are run for comparison. The results from the numerical simulations using the BBM implemented within both the single phase and the mixture multiphase frameworks are compared with the results from the rig tests in Fig. 10. The results show comparison of local metal temperature in the vicinity of the exhaust valve bridge of all four cylinders. Based on the data available from the tests in the vicinity of the exhaust valve bridge, the inaccuracy in measurement due to an uncertainty of 1 mm in positioning the thermocouple probes is estimated. The details of this uncertainty analysis are elaborated in by Båstedt et al. [18]. These measurement inaccuracies are presented as error bars in Fig. 10. The results from the simulations are in reasonably good agreement with the measurement. The coolant flow passage in the exhaust valve bridge is designed to ensure high coolant flow rate. Thereby, the difference between the temperature values from the single phase and the mixture multiphase frameworks is marginal. This is also in line with the results from the simulations for the channel flow.

Fig. 11 shows local metal temperature vs. coolant pressure plots measured in 'Position 1' in the exhaust flange (in contrast to Fig. 9 which applies to the exhaust valve bridge), indicated in Fig. 7(b). As observed in the exhaust valve bridge region, for 100% coolant flow rate, the occurrence of boiling is evidenced by a decrease in local metal temperature with decrease in coolant pressure. However, reducing the coolant flow rate to 80%, the temperature decreases with reduction in pressure until a certain value of pressure and thereafter increases with further reduction in pressure. This is interpreted as the occurrence of transition boiling. The reduced heat transfer characteristics in the transition boiling regime causes the increase in local metal temperature. With further reduction in coolant flow rate to 60%, this behavior is observed for even higher values of coolant pressure. Similar behavior

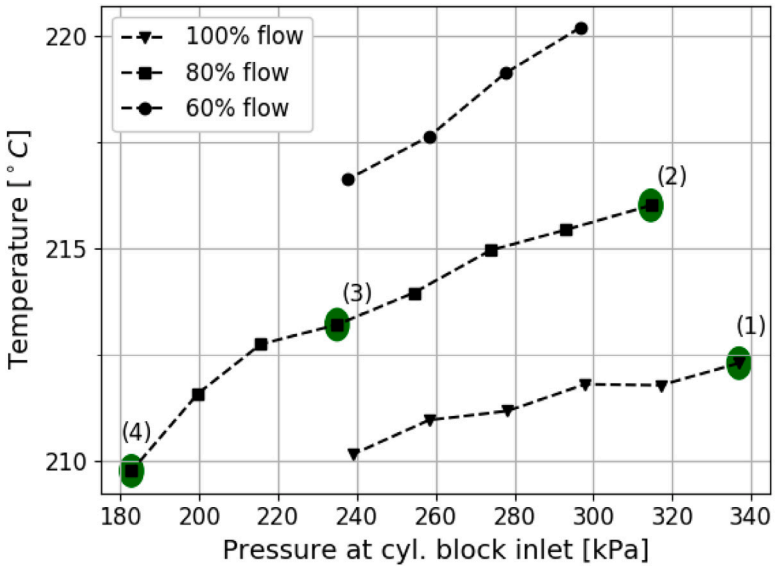


**Fig. 9.** Example of local metal temperature vs. coolant pressure in the exhaust valve bridge region of Cylinder 4. Coolant bulk temperature at the inlet is 100 °C. Selected operating conditions, for which results from numerical simulations are presented in Fig. 10, are also marked.

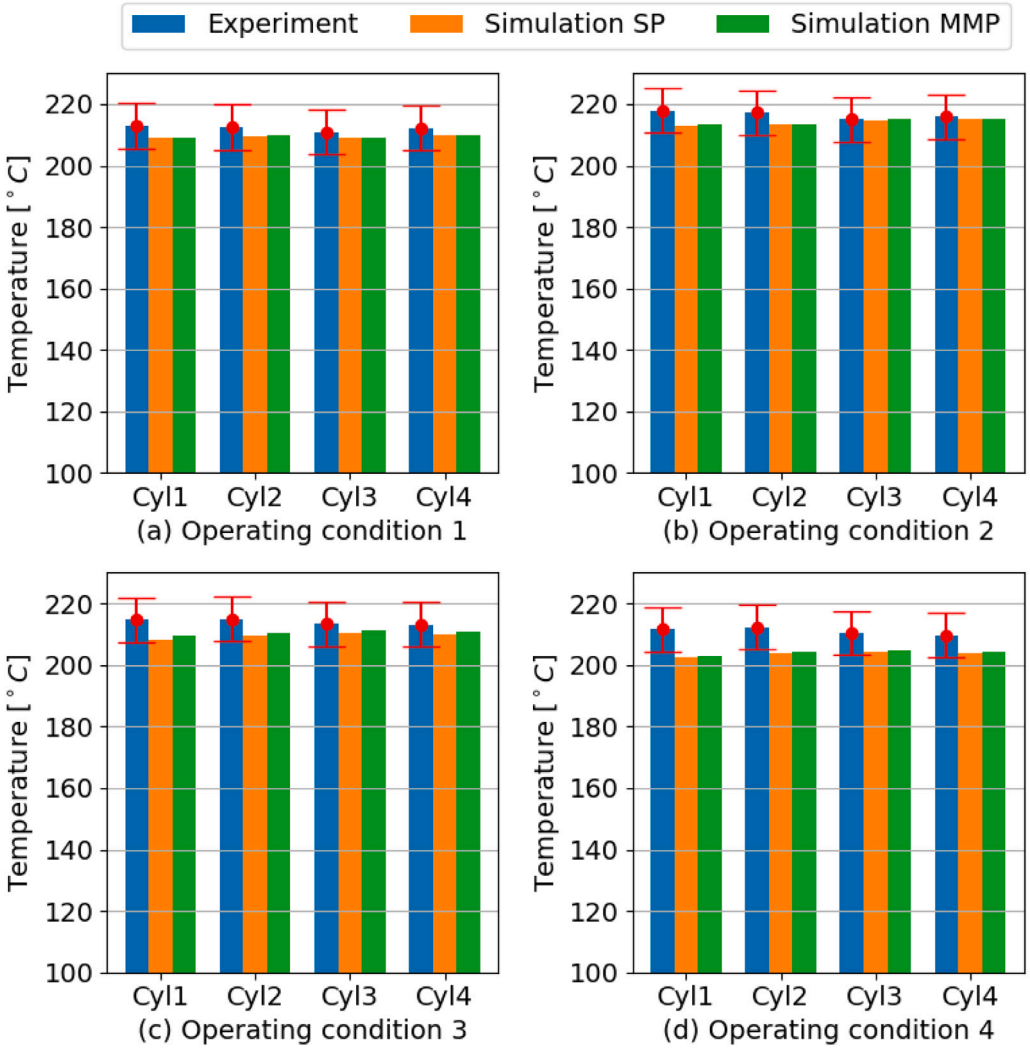


**Fig. 10.** Comparison of local metal temperature obtained from engine rig tests (Experiment), Single phase numerical simulations (Simulation SP) and mixture multiphase numerical simulations (Simulation MMP), in the vicinity of the exhaust valve bridge of all four cylinders. The selected operating conditions are the ones marked in Fig. 9. Coolant bulk temperature at the inlet is 100 °C.

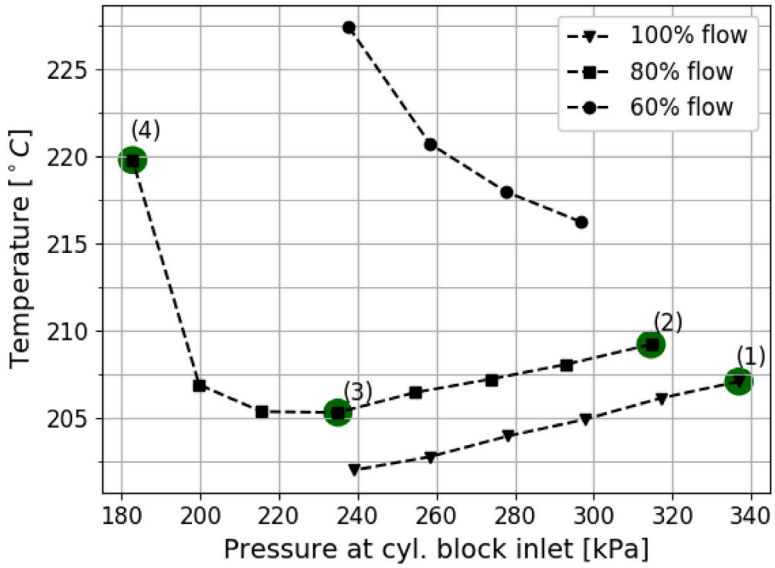


**Fig. 11.** Example of local metal temperature vs. coolant pressure measured at Position 1 in the exhaust flange region. Coolant bulk temperature at the inlet is 100 °C. Selected operating conditions, for which results from numerical simulations are presented in Fig. 12, are also marked.

is observed in 'Position2' and 'Position3'. The four operating conditions for which the numerical simulations are run are marked in Fig. 11.

Temperature in the vicinity of the exhaust flange obtained from the numerical simulations are compared with measurement and presented in Fig. 12. Although the flow velocities are much lower in the vicinity of the exhaust flange, compared to the exhaust valve bridge region, the difference between the single phase and multiphase simulations are still marginal, especially in operating conditions 1 and 2. A consistent over-prediction of temperature by the numerical simulations has been observed at Position 2 for the operating conditions 1, 2 and 3. For these operating conditions, the agreement in Position 1 and 3 is reasonably good. For operating condition 4, the temperature is under-predicted significantly. In other words, the heat transfer is over-predicted. As discussed previously, operating condition 4 is interpreted to be in the transition boiling regime. The BBM, which accounts for the boiling heat flux at the fluid–solid interface, is indeed not intended to handle transition boiling. The model is only intended to better capture the development from incipient to fully developed boiling, which are the boiling regimes relevant for application in internal combustion engines. A value of $\Pi$ asymptotically approaching 1 informs the occurrence of FDB and, thereby, inherently sets the limit for its own applicability. The model is not intended to be used to estimate the wall heat flux once this limit is attained. Furthermore, the difference between the temperatures from the single phase and the mixture multiphase frameworks is relatively high in operating conditions 3 and 4 compared to 1 and 2. This is due to the higher boiling intensity and the consequent higher vapor generation.

As mentioned previously, the BBM estimates the probability of interaction, $\Pi$, between vapor bubbles created during the boiling process where a value of $\Pi \simeq 1$ indicates the occurrence of fully developed boiling. The probability itself can be used to estimate the local extent of boiling and can be used as a threshold to apply as a practical limit during engine design. In Fig. 13 the probability of bubble interaction, predicted by the mixture multiphase framework, is shown as a contour plot in spherical observation regions close to the probe locations. As can be seen, $\Pi \simeq 1$ is predicted for Operating conditions 3 and 4, while much lower values are reported for the other two operating conditions.

Although the computed local metal temperature in different probe locations are quite similar in the single phase and multiphase frameworks, a difference in distribution of probability of bubble interaction is observed. Fig. 14 shows the contour of probability of bubble interaction, $\Pi$, in the IEM region (indicated in Fig. 8) using both the single phase and multiphase frameworks for operating condition 3. The IEM is characterized by low coolant velocities and therefore experiences significantly more boiling compared to the exhaust valve bridge. As a result of this, in the single phase framework, the liquid temperature in the near wall region increases beyond its saturation temperature and in some locations equals the wall temperature. This causes the suppression factor, shown in Eq. (25), to limit the boiling heat flux and thereby also limit the heat transfer from the wall. As a consequence, the wall temperature increases, which in turn increases the wall superheat ($T_{wall} - T_{sat}$). The active nucleation site density and, therefore, the probability of bubble interaction are directly proportional to the wall superheat, as shown in Eq. (30). Therefore, the single phase framework estimates larger regions experiencing $\Pi \simeq 1$ in the IEM. The multiphase framework does not have a suppression factor, since it accounts for the presence of the vapor phase. Hence, the heat transfer from the wall is not arbitrarily limited. The estimated wall temperature and the values of wall superheat are more accurate. Therefore, the probability of bubble interaction is also more accurate. In other words, while the single phase framework predicts occurrence of fully developed boiling in a particular region conservatively, the multiphase framework more accurately identifies the specific vicinity inside the region where fully developed boiling is actually encountered. This deeper analysis, made available by the probability $\Pi$, clearly shows the advantage of using the multiphase framework, which accounts for the presence of the vapor phase and thereby resolves more physics involved in subcooled boiling flow.

In the discussions regarding the channel flow case, it is indicated that extensive grid refinement does not give accurate results when using the mixture multiphase framework. The contours of wall $y^+$ on the coolant jacket are shown in Fig. 15 for operating condition 3. The mesh resolution is such that wall functions are always used in the flame deck region, especially in the exhaust valve bridge. Resolving the viscous sublayer could not be avoided in the Integrated Exhaust Manifold, IEM, region due to uneven flow distribution in the coolant jacket in this region. Although the values of wall $y^+$ are quite low, locally in certain regions of the coolant jacket in the IEM, the agreement of the local metal temperature in the IEM region, i.e., in the vicinity of the exhaust flange is in reasonably good agreement with the measurements. From this, it is evident that the mixture multiphase framework and the BBM can be used for applications involving complex geometries without significant loss of accuracy.

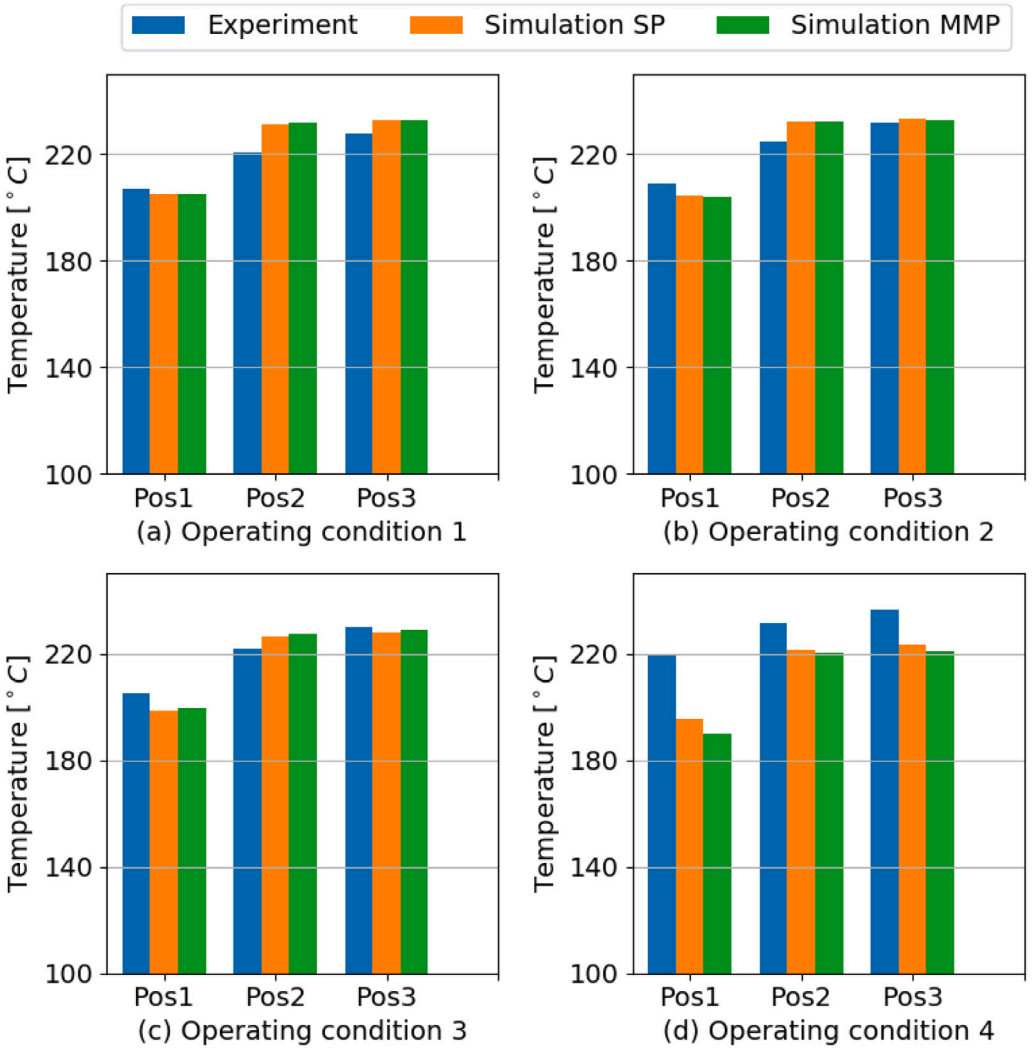


**Fig. 12.** Comparison of local metal temperature obtained from engine rig tests (Experiment), Single phase numerical simulations (Simulation SP) and mixture multiphase numerical simulations (Simulation MMP), in the vicinity of the exhaust flange. The selected operating conditions are the ones marked in Fig. 11. Coolant bulk temperature at the inlet is 100 °C.

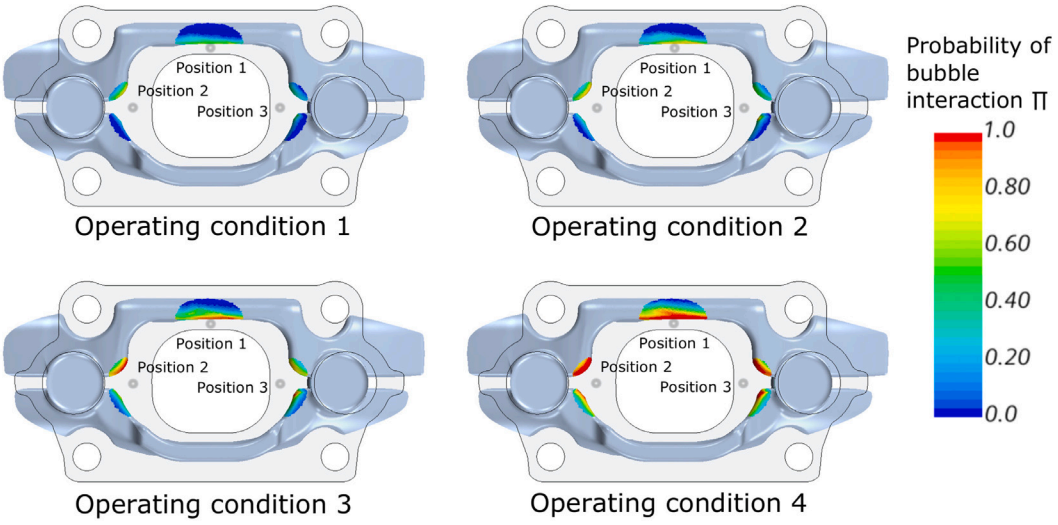


**Fig. 13.** Probability of bubble interaction, $\Pi$, predicted using the mixture multiphase framework in the vicinity of probes in the exhaust flange region.

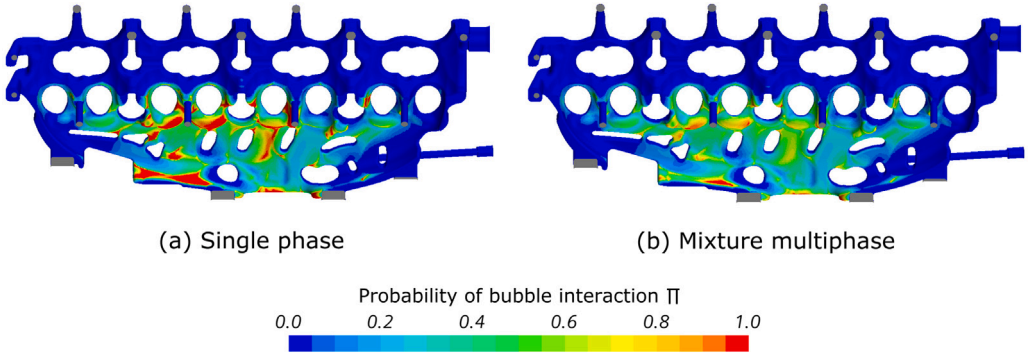


**Fig. 14.** Probability of bubble interaction, $\Pi$, predicted using the single phase and the mixture multiphase frameworks in the coolant jacket in vicinity of the IEM (shown in Fig. 8).

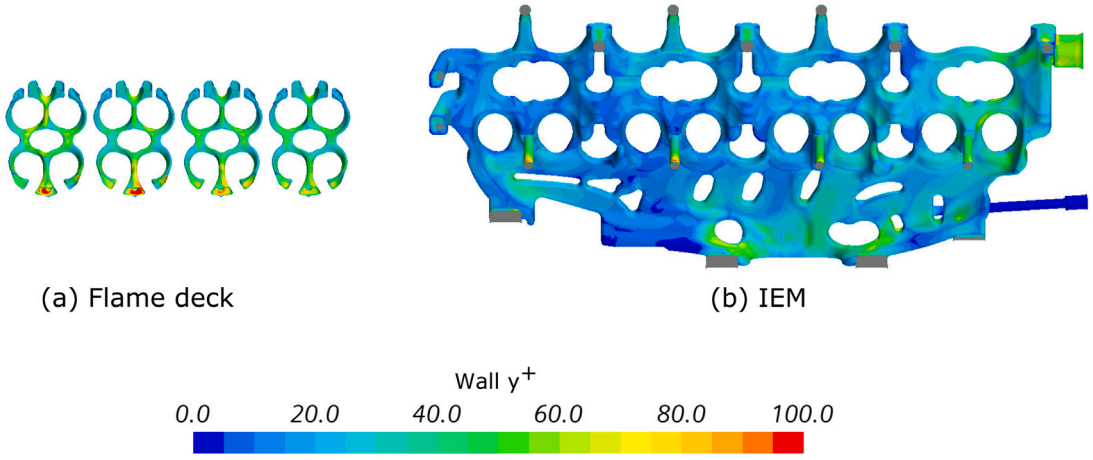


**Fig. 15.** Wall $Y^+$ on the surface of the coolant jacket close to the (a) flame deck and (b) IEM regions.

## 4. Conclusion

This article presents a comparative study between single phase and mixture multiphase simulation frameworks for analysis of flows with vapor generated by nucleate boiling. The Blended Boiling Model proposed by Vasudevan et al. [9] is used in the study. The application in focus is the coolant jacket in internal combustion engines. In the first part, subcooled flow boiling in a channel flow is studied by comparing the simulation results with experiments by Steiner et al. [10]. The single phase framework gives good results for all cases tested except the one with a very low coolant flow rate. On account of the low coolant flow rate, the intensity of boiling and thereby the net vapor generation is higher, compared with the other cases. Therefore, accounting for the presence of the vapor phase using the multiphase framework gives results with closer agreement to the measurements for this test case. Furthermore, it is found that excessive grid refinement leads to inaccurate results in both the single phase and the mixture multiphase frameworks. The use of wall functions is recommended in this regard. A detailed grid sensitivity analysis is performed for the mixture multiphase framework in support of the argument.

In the second part, subcooled boiling flow in a four-cylinder petrol engine is analyzed using both the single phase and multiphase frameworks. Four operating conditions are chosen from the rig tests and the simulation results for these conditions are compared with the measurement data. The computed values of local metal temperature are in good agreement with the measured values in the exhaust valve bridge region. Since this region is designed to have high coolant flow velocity, the net vapor generated is low. Hence the difference between the single phase and multiphase simulation results is small, as in the channel flow case. The most critical region from the point of view of boiling is in the vicinity of the exhaust flange. For operating conditions with low coolant flow rate and low system pressure, occurrence of transition boiling is evidenced from the measured data of local metal temperature. One of the four operating conditions chosen for numerical simulation is in the transition boiling regime, meaning in a regime with vapor concentration at the liquid–solid interface high enough to significantly reduce heat transfer. The BBM estimates the probability of bubble interaction, $\Pi$, which indicates the occurrence of fully developed boiling. A value of $\Pi \simeq 1$ is estimated for operating conditions 3 and 4, indicating the occurrence of fully developed boiling. Although there is no further information about proximity to critical heat flux and occurrence of transition boiling, a value of $\Pi \ll 1$, with sufficient margin from the asymptotic limit of $\Pi \simeq 1$, is suggested to be used as a limit for safe operation of practical engineering applications, such as the engine coolant jacket. The local metal temperature in operating condition 4 is under-predicted by the numerical simulations. Notably the BBM is not intended to be applied in such regimes and these results confirm this limitation. Furthermore, while comparing the contours of $\Pi$ obtained from the single phase and multiphase frameworks, it is noticeable that the single phase framework is more conservative in indicating regions experiencing excessive boiling.

From the point of view of an engine designer, the single phase simulation framework is a powerful tool, given the lower computational costs. It estimates the temperature in critical regions with reasonably good accuracy and indicates regions experiencing excessive boiling with a larger margin of safety. However, with the need for more advanced cooling strategies in high specific power engines, tapping the potential of controlled nucleate boiling is a viable option. This necessitates simulation frameworks, such as the mixture multiphase

framework, that resolve more of the physics involved in the phenomenon of boiling and estimate the upper limit for safe boiling with better accuracy, while staying economical in terms of computational costs.

## CRediT authorship contribution statement

**Sudharsan Vasudevan:** Conceptualization, Methodology, Validation, Formal analysis, Writing – original draft, Visualization. **Sassan Etemad:** Conceptualization, Methodology, Writing – review & editing, Supervision, Project administration, Funding acquisition. **Lars Davidson:** Methodology, Resources, Writing – review & editing, Supervision. **Mirko Bovo:** Methodology, Resources, Writing – review & editing, Supervision.

## Declaration of competing interest

The authors declare that they have no known competing financial interests or personal relationships that could have appeared to influence the work reported in this paper.

## Data availability

Data could be made available on request, depending on the confidentiality.

## Acknowledgment

The authors are grateful to Energimyndigheten (Swedish Energy Agency) for the financial support.

## References

[1] Shiyang Hua, Ronghua Huang, Pei Zhou, Numerical investigation of two-phase flow characteristics of subcooled boiling in IC engine cooling passages using a new 3D two-fluid model, Appl. Therm. Eng. 90 (2015) 648–663.
[2] N. Kurul, Michael Z. Podowski, Multidimensional effects in forced convection subcooled boiling, in: International Heat Transfer Conference Digital Library, Begel House Inc., 1990.
[3] Tao Bo, CFD Homogeneous Mixing Flow Modelling to Simulate Subcooled Nucleate Boiling Flow, Technical Report, SAE Technical Paper, 2004.
[4] Warren M. Rohsenow, A Method of Correlating Heat Transfer Data for Surface Boiling of Liquids, Technical Report, Cambridge, Mass.: MIT Division of Industrial Cooporation, 1951.
[5] V. Pržulj, M. Shala, Multi-phase mixture modelling of nucleate boiling applied to engine coolant flows, in: Computational Methods in Multiphase Flow V, vol. 63, WIT Press, 2009, pp. 135–146.
[6] Mehmet Shala, Simulation of nucleate boiling flow using a multiphase mixture modelling approach, IMA J. Appl. Math. 77 (1) (2012) 47–58.
[7] Hemant Punekar, Saurish Das, Numerical Simulation of Subcooled Nucleate Boiling in Cooling Jacket of IC Engine, Technical Report, SAE Technical Paper, 2013.
[8] Saurish Das, Hemant Punekar, On development of a semimechanistic wall boiling model, J. Heat Transfer 138 (6) (2016).
[9] Sudharsan Vasudevan, Sassan Etemad, Lars Davidson, Gonzalo Montero Villar, Numerical model to estimate subcooled flow boiling heat flux and to indicate vapor bubble interaction, Int. J. Heat Mass Transfer 170 (2021) 121038.
[10] Helfried Steiner, Alexander Kobor, Ludwig Gebhard, A wall heat transfer model for subcooled boiling flow, Int. J. Heat Mass Transfer 48 (19–20) (2005) 4161–4173.
[11] Siemens Digital Industries Software, Simcenter STAR-CCM+ user guide v. 2020.3, 2020.
[12] H.K. Forster, Novak Zuber, Dynamics of vapor bubbles and boiling heat transfer, AIChE J. 1 (4) (1955) 531–535.
[13] Quan Li, Yongjun Jiao, Maria Avramova, Ping Chen, Junchong Yu, Jie Chen, Jason Hou, Development, verification and application of a new model for active nucleation site density in boiling systems, Nucl. Eng. Des. 328 (2018) 1–9.
[14] Prof. Helfried Steiner, Institute of Fluid Mechanics and Heat Transfer, Graz University of Technology, Austria, Personal communications.
[15] F.W. Dittus, L.M.K. Boelter, University of California Publications on Engineering, 2, 1930, p. 371.
[16] K. Robinson, J.G. Hawley, N.A.F. Campbell, Experimental and modelling aspects of flow boiling heat transfer for application to internal combustion engines, Proc. Inst. Mech. Eng. D 217 (10) (2003) 877–889.
[17] I.C. Finlay, D. Harris, D.J. Boam, B.I. Parks, Factors influencing combustion chamber wall temperatures in a liquid-cooled, automotive, spark-ignition engine, Proc. Inst. Mech. Eng. D 199 (3) (1985) 207–214.
[18] P. Båstedt, S. Vasudevan, M. Bovo, Subcooled flow boiling in high power density internal combustion engines I: Thermal survey measurement campaign, SAE Int. J. Engines 16 (1) (2023) http://dx.doi.org/10.4271/03-16-01-0002.